

An Independent Planet Search In The Kepler Dataset

II. An extremely low-density super-Earth mass planet around Kepler-87.

Aviv Ofir^{1,2}, Stefan Dreizler¹, Mathias Zechmeister¹, and Tim-Oliver Husser¹

¹ Institut für Astrophysik, Georg-August-Universität, Friedrich-Hund-Platz 1, 37077 Göttingen, Germany.

² e-mail: avivofir@astro.physik.uni-goettingen.de

Received XXX; accepted YYY

ABSTRACT

Context. The primary goal of the *Kepler* mission is the measurement of the frequency of Earth-like planets around Sun-like stars. However, the confirmation of the smallest of *Kepler*'s candidates in long periods around FGK dwarfs is extremely difficult or even beyond the limit of current radial velocity technology. Transit timing variations (TTVs) may offer the possibility for such confirmations of near-resonant multiple systems by the mutual gravitational interaction of the planets.

Aims. We previously detected the second planet candidate in the KOI 1574 system. The two candidates are relatively long-period (about 114d and 191d) and in 5:3 resonance. We therefore search for TTVs in this particularly promising system.

Methods. The full *Kepler* data was detrended with the proven SARS pipeline. The entire data allowed searching for TTVs of the above signals, as well as searching for additional transit-like signals.

Results. We detect strong anti-correlated TTVs of the 114d and 191d signals, dynamically confirming them as members of the same system. Dynamical simulations reproducing the observed TTVs allow us to also determine the masses of the planets. KOI 1574.01 (hereafter Kepler-87 b) was found to have a radius of $13.49 \pm 0.55 R_{\oplus}$ and a mass of $324.2 \pm 8.8 M_{\oplus}$, and KOI 1574.02 (Kepler-87 c) was found to have a radius of $6.14 \pm 0.29 R_{\oplus}$ and a mass of $6.4 \pm 0.8 M_{\oplus}$. Both planets have low densities of 0.729 and $0.152 g cm^{-3}$, respectively, which is non-trivial for such cold and old (7-8 Gyr) planets. Specifically, Kepler-87 c is the lowest-density planet in the super-Earth mass range. Both planets are thus particularly amenable to modeling and planetary structure studies, and also present an interesting case where ground-based photometric follow-up of *Kepler* planets is very desirable. Finally, we also detect two more short-period super-Earth sized planetary ($< 2 R_{\oplus}$) candidates in the system, making the relatively high multiplicity of this system notable against the general paucity of multiple systems in the presence of giant planets like Kepler-87 b.

Key words. methods: data analysis – stars: planetary systems

1. Introduction

It is very difficult to detect, and even more difficult to confirm, small planets orbiting in long periods around their host star – where the liquid-water habitable zone (HZ) resides. This is relatively easier for M dwarf host stars since they are both smaller and lighter than Sun-like stars, making the respective transit and radial velocity signals larger. These considerations, coupled with the M dwarfs prevalence in the stellar population, are behind the great interest in M dwarfs and their HZ planets (e.g. Anglada-Escudé *et al.* 2012). However, for more massive stars, like the Sun and the bulk of the *Kepler* target stars, small HZ planets remain elusive targets. The few small HZ planets that were detected so far (e.g. Kepler-22, Borucki *et al.* 2012) are all either around M dwarfs or with no dynamical confirmation (i.e., no mass measured). One way to positively detect such objects is using transit timing variations: in near-resonant systems the amplitude of these variations can allow detecting small planets, even down to Earth-mass, in *Kepler*'s data (Holman & Murray 2005).

KOI 1574 was flagged in Batalha *et al.* 2013 as having a relatively deep ($\sim 0.5\%$) candidate with a period of $P_{01} \approx 114d$ (hereafter KOI 1574.01). Ofir & Dreizler (2013, hereafter OD13) re-analyzed all of *Kepler*'s KOIs and found 84 new transiting planets candidates in these light curves. Among them, OD13 identified an additional candidate in the KOI 1574 system using quarters 0 through 6 data. The additional outer candidate is in 5:3 resonance with KOI 1574.01, or a period of $P_{02} \approx 191d$

(hereafter also KOI 1574.02). In this work we describe the KOI 1574 planetary system, and KOI 1574.02 in particular, as the first detection of a transiting super-Earth mass in a long period (near the HZ of KOI 1574). We present the spectral analysis of the host star on §2, light curve processing on §3, the observed TTVs and the resultant derived masses on §4, and conclude.

2. Spectral analysis

2.1. Observed spectra

We used two spectra of KOI 1574 for spectral analysis. The first one has been downloaded from the Kepler Community Follow-up Observing Program (CFOP) website ¹. The spectrum was taken by Erik Brugamyer and William Cochran using the (Tull) Coude spectrograph at the 2.7 meter (Harlan J. Smith) telescope at the McDonald Observatory on JD 2455703.83350 with an exposure time of 2900 sec. The spectrograph has a resolution of 60 000 and covers a spectral range from about 3750 Å up to 10 000 Å. The useful range is however restricted to 4250-9000 Å due to low signal-to-noise outside this range. The spectrum has been reduced with IRAF applying standard processing.

The second spectrum has been taken with the Hobby Eberly Telescope (HET; Ramsey *et al.*, 1998) with the High Resolution Spectrograph (HRS; Tull *et al.*, 1995) in a setup (15k central

¹ <https://cfop.ipac.caltech.edu/home/>

600g5271 2as 2sky IS0 GC0 2x5) which provides a resolution of 15 000 and a wavelength coverage from 4260 Å to 6220 Å. It has been obtained on 2012-09-23 (JD = 2456193.705981) with an exposure time of 2400 sec. Using the IDL based REDUCE package (Piskunov & Valenti, 2002) the spectrum was bias corrected, flat-fielded, optimally extracted, and finally wavelength calibrated using a ThAr lamp.

2.2. Model atmosphere fitting

At the Kepler-CFOP web page Sam Quinn provided the following analysis for the McDonald coude spectrum: $T_{\text{eff}}=5750$ K, $\log(g) = 4.0$, $V_{\text{rot}}=4$ km/s at solar metallicity. It has to be noted that the uncertainties are estimated to be ± 125 K, ± 0.25 dex, and ± 1 km/s for the effective temperature surface gravity and rotational velocity. Due to the correlation between metallicity and effective temperature, a variation of the metallicity by 0.2 dex would result in an additional uncertainty of the the effective temperature of about 200 K. From a comparison of these values with stellar evolution models, the mass determination of the central star would be uncertain by 20-30%.

In order to improve the parameter determination we performed a model atmosphere fitting using the newest PHOENIX model grid (Husser *et al.* 2012). Models are available in steps of 100 K, 0.5 dex, and 0.5 dex in effective temperature, surface gravity and metallicity. The microturbulence is not a free parameter but is derived from a scaling law using the mean convective velocity with each model. This scaling relation has been calibrated using 3D radiative transport on 3D hydrodynamical simulations. Other improvements compared to earlier models is a new equation of state as well as spherical symmetry for all models. We use a Levenberg-Marquardt optimization to fit the effective temperature, surface gravity, metallicity, and rotational velocity (only in the higher resolved McDonald spectrum) simultaneously with a polynomial for the continuum for each spectral order. The surface gravity, however, was allowed to vary in a small interval $\log(g)=[3.9,4.0]$ only, which can be derived from the ratio of the stellar radius and the orbital period of the planet taken from the light curve analysis (§3), Kepler’s Third Law, and stellar evolution models. The final values and errors are weighted means over all spectral orders. It should be noted that we multiplied the errors by a factor of two in order to account for systematic errors, e.g. from the fact that the model atmospheres have to be calculated in 1D, allowing to treat convection only in the mixing length approximation, or from the fact that the instrumental broadening was approximated with a Gauss-profile.

The stellar parameters determined from the two spectra (see Table 1 and also Fig. 1) marginally agree within their 1σ errors. For the final stellar parameters we adopt a mean from the two determinations. The parameters reported in CFOP reveal a slightly higher effective temperature. It should be noted that a solar abundance was assumed in that case. With our slightly sub-solar metallicity a somewhat lower effective temperature is needed to achieve similar line strengths of the mainly neutral metal lines.

We use the stellar parameters to compare KOI 1574 with Padova stellar evolution models (mass fraction for hydrogen $X = 72.3\%$, Helium 26% and metals $Z = 1.7\%$; (Bertelli *et al.* 2008)) as well as with Y^2 models (mass fraction for hydrogen $X = 71\%$, Helium 27% and metals $Z = 2\%$ (Yi *et al.* 2001, Kim *et al.* 2002, Yi, Kim, & Demarque 2003, Demarque *et al.* 2004)). KOI 1574 is a star at the end of its main sequence phase. The slightly sub-solar metallicity is consistent with an age of

	McDonald	HET	mean
Resolution	60 000	15 000	
T_{eff} [K]	5550 ± 60	5640 ± 45	5600 ± 50
$\log(g)$ [cgs]	3.95 ± 0.02	3.96 ± 0.02	3.96 ± 0.02
[Fe/H]	-0.18 ± 0.04	-0.16 ± 0.03	-0.17 ± 0.03
V_{rot} [km/s]	4.3 ± 0.2	fixed	4.3 ± 0.2

Table 1. Stellar parameters derived from our model atmosphere fit for the McDonald 2.7m spectrum and the HET High Resolution Spectrograph. It should be noted that the surface gravity was allowed to vary in a small interval determined by the stellar density derived from the light curve fits only.

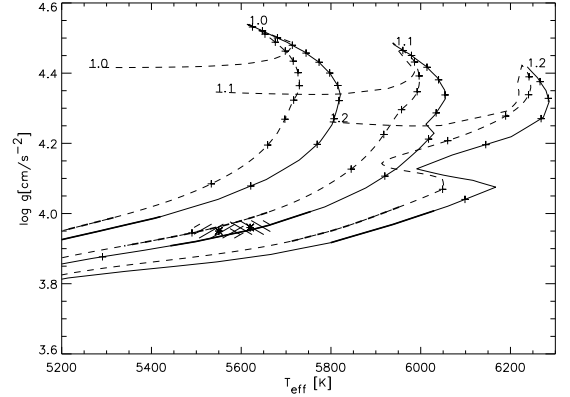


Fig. 1. Stellar parameters from Table 1 (shaded area) compared to Padova stellar evolution models (solid line) and Y^2 models (dashed line). Note that the models differ slightly in their chemical composition. The bold regions on the tracks indicate the ratio of the stellar radius to the semi major axis of the planetary orbit derived from its orbital period, the mass of the stellar model, and Kepler’s Third Law. The “+” symbols indicate 1Gyr time steps.

about 7-8 Gyr. We derive a stellar mass of $1.1 M_{\odot} \pm 0.05 M_{\odot}$, which takes into account the dependence of the chemical composition as well as possible systematic errors in the evolution models. This results in a stellar radius of $1.82 R_{\odot} \pm 0.04 R_{\odot}$.

3. Light curve analysis

3.1. Preprocessing and detection

We use the full Kepler data – quarters 1 through 16 – in our analysis. The additional data includes a few more transits of KOI 1574.01 relative to OD13, and importantly - the third and fourth transit events of KOI 1574.02 (unfortunately the star fall on the inactive Module 3 during Quarters 7, 11 and 15 and transits that did occur were not observed). We applied nearly the same processing as in OD13 to the entire dataset. In short, it includes the removal of long-term trends by the application of a median filter to each continuous section individually, and the identification and removal of both additive and relative systematic effects in the data simultaneously with the SARS algorithm (Ofir *et al.* 2010). The only differences were: (a) the inclusion of a correction for crowding and flux ratio effects as in eq. 2 of Stumpe *et al.* (2012), (b) the use of the newly-available target-specific status indicator to identify continuous sections instead of a global anomaly table, and (c) active avoidance of variable stars (KOIs, eclipsing binaries and red giants) from the SARS learning set.

We re-searched the KOI 1574 system for transit signals and found the previous two signals very significantly. We then

searched for transit time variations (TTVs) for each signal by fitted the linear-ephemeris model (computed using the Mandel and Agol (2002) formalism) to each one of the individual transits, allowing only for the time of mid-transit to vary. Indeed, KOIs 1574.01 and 1574.02 show strongly anti-correlated TTVs (see Fig. 3 and discussion on §4). These anti-correlated TTVs, coupled with the dynamical simulations that give strong limits on the masses of the two objects, allow us to dynamically confirm the KOIs 1574.01 and 1574.02 signals as true planets in the same planetary system. We therefore name these planets Kepler-87 b and c, respectively.

After the above initial TTVs-corrected modeling we modeled-out the planets and re-calculated the background long-term trends and re-fitted the planets – till convergence. We then removed the Kepler-87 b and c models completely and applied the Optimal Box Least Squares technique (Ofir 2013) to search for additional transit signals in the residuals, and detected two additional short-period transit-like signals with periods of $P_{03} \approx 5.83\text{d}$ and $P_{04} \approx 8.97\text{d}$ above the 7.1σ significance threshold – hereafter KOI 1574.03 and KOI 1574.04, respectively. We note that the 1574.03 signal was also identified by the Kepler team in the Q0-Q8 data². The new signals also passed all the other tests described in OD13. Actually, At this point we custom-fitted the long-term filter for this particular object: we changed the general segmented median filter to a segmented Savitzky-Golay filter (Savitzky & Golay 1964) (of second order, in a two-days window span) with iterative 3σ clipping, which is better than a simple median filter, and repeated all the above. We note that KOI 1574.03 and KOI 1574.04 show no significant TTVs - but the error bars are quite large for such shallow and short-period candidates.

3.2. Global fit

We derived the final system parameters (given in Tables 2 and 4, illustrated in Fig. 2) by simultaneously fitting all four signals. We iterated the procedure below and the background long-term trends fitting several times till convergence, and report the final iteration here. We used circular orbits for all signals, but we allowed the phase of all Kepler-87 b & c transits to be set relative to the closest time of mid-transit, and optimized for these times as well. This perturbed-circular fit is valid in the small TTVs regime only, and indeed the largest TTVs detected are about $7.5 \cdot 10^{-5}$ of P_{01} and $6 \cdot 10^{-4}$ of P_{02} . The scaled semi-major axis a/R_* parameter was common to all candidates: as in OD13 we scaled it by Kepler’s third law for each candidate. The final fit therefore included these parameters: one a/R_* , four planet radii r_p/R_* , four impact parameters b_p/R_* , eleven T_{mid} for Kepler-87 b, four T_{mid} for Kepler-87 c, and two linear parameters (P and T_{mid}) for each of KOIs 1574.03 and 1574.04 - a total of 28 floating parameters. Once initial results suggested the proximity of Kepler-87 c to the HZ (below), and since the relevant parameter a/R_* is usually both the most difficult to fit (has the largest error) and may have some sensitivity to the initial starting point, we ran twelve $5 \cdot 10^5$ -step MCMC fits that allowed all the variables to float – each with a different a/R_* starting points evenly sampled between half and twice our initial estimate. We then checked that all twelve parameters sets converges on consistent values to 1σ on all parameters. The total of the 12 chains exhibited a smooth distribution of values up to $\Delta\chi^2 < 100$ (relative to the global minimum) so we considered as “burn-in” of each

² As cataloged at the Exoplanet Archive <http://exoplanetarchive.ipac.caltech.edu/index.html>

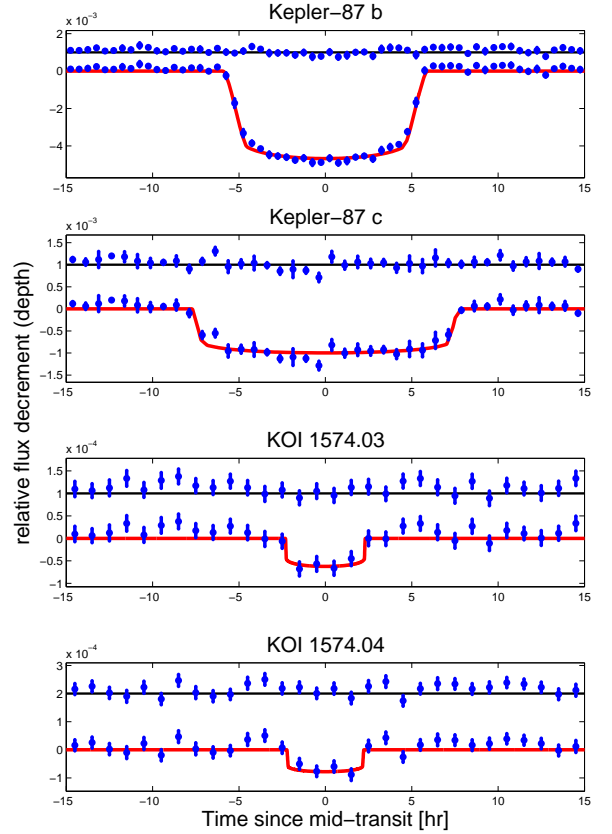


Fig. 2. Phased and binned (to half-hour bins) light curves of the Kepler-87 system components relative to the time of mid transit, with over plotted best-fitting models. From top to bottom: transiting exoplanets Kepler-87 b and c and planetary candidates KOIs 1574.03 and 1574.04. Above each light curve we show the model residuals, shifted for clarity. Note the vertical scale in each panel may be different.

MCMC chain as all the steps before the first time $\Delta\chi^2 < 100$ was reached, relative to the global minimum, and concated all these truncated chains (as in Tegmark *et al.* 2004) to one very large, nearly $6 \cdot 10^6$ steps long, chain that was used for parameter estimation. The final linear ephemeris for Kepler-87 b and c and their error bars were computed from the distribution of fits to the different T_{mid} along the MCMC chain. We note that the final a_{01}/R_* is smaller than the linear one (given in OD13), as expected: the linear ephemeris fit caused the average signal to appear smeared, and therefore with artificially higher a_{01}/R_* .

The equilibrium temperature of exoplanet Kepler-87 c is mostly derived from the above model’s a/R_* axis and the host star T_{eff} using:

$$T_{eq} = T_{\text{eff}} \left(\frac{R_*}{2a} \right)^{1/2} [f(1 - A_B)]^{1/4} \quad (1)$$

However, the planetary atmospheric parameters flux redistribution factor f and Bond albedo A_B are completely unknown, and have a large effect on the resultant T_{eq} . “Conventional” values would assume efficient redistribution of the stellar flux

Table 2. Timing results of the perturbed circular orbit fit for the Kepler-87 b and Kepler-87 c planets. Residuals are calculated relative to the best-fit linear solution.

Best-fit time of mid transit (BJD-2454833)	Median time of mid transit (BJD-2454833)	Residuals from linear ephemeris [d]	1 σ error [d]
Kepler-87 b			
165.1564	165.1576	0.0056	+0.0025
279.8881	279.8884	0.0001	-0.0024
394.6166	394.6161	-0.0086	± 0.0017
509.3531	509.3527	-0.0083	± 0.0016
624.1031	624.1034	0.0060	± 0.0014
738.8414	738.8409	0.0071	+0.0014
853.5690	853.5700	-0.0001	+0.0015
968.3024	968.3010	-0.0055	+0.0018
1197.7846	1197.7845	0.0053	-0.0017
1312.5218	1312.5223	0.0068	± 0.0020
1541.9800	1541.9798	-0.0085	± 0.0015
Kepler-87 c			
286.0894	286.0900	-0.1606	+0.0059
477.6302	477.6292	0.1467	-0.0069
860.0537	860.0483	0.1022	+0.0051
1242.3155	1242.3152	-0.0945	-0.0053

Table 3. Predicted transit times for the Kepler-87 b and c planets for the next few years of the adopted model.

Predicted time of mid transit (BJD-2454833)					
Kepler-87 b			Kepler-87 c		
1312.521	1771.462	2230.386	2574.589	1434.256	2200.750
1427.251	1886.196	2345.130	2689.316	1625.957	2391.878
1541.980	2000.924	2459.862	2804.046	1816.789	2584.208
1656.714	2115.653	2459.862	3033.517	2008.904	2776.229

($f = 1$) and Earth-like albedo ($A_B=0.3$), and these lead to $T_{eq,02}=403.3$, or just hotter than the inner edge of the habitable zone. However, f and A_B are completely unknown and can vary considerably. Such changes in any of f or A_B can lower the $T_{eq,02}$ to well within the HZ.

4. Transit timing variations

Fig. 3 shows the observed TTVs for Kepler-87 b and c with their error bars (relative to linear ephemeris). A search for the best-fitting sine for the TTVs of Kepler-87 b (which has enough data points to perform such an analysis), gave a single peak with a super-period of 514^{+38}_{-80} d, which agrees with the expected $5 \times P_{01} = 573.69$ to 1.5σ , further showing that the TTVs are indeed caused by the interaction between Kepler-87 b and c. Finally, one can prove that these TTVs are indeed from planet-planet interaction by looking for anti-correlation between the TTVs of Kepler-87 b and c (Ford *et al.* 2012, Steffen *et al.* 2012 and Fabrycky *et al.* 2012), and indeed they exist, and this means that: (a) Kepler-87 b and Kepler-87 c are indeed interacting planets in the same system, and (b) we can try to determine the masses of both planets.

We used the hybrid symplectic integrator within the *Mercury* package (Chambers 1999), which we have run with a constant time step of 0.5 days, i.e. less than 1% of the orbital period of the P_{01} planet. We assume co-planar orbits, well justified from the transit fitting (see Table 4), which together with the stellar and the two planetary masses result in 11 free parameters for the 15 measured transit timings. The two inner planet candidates

Table 4. Observed and derived parameters for the Kepler-87 (KOI 1574) system. Subscript XX is understood to be the relevant parameter for signal 1574.XX. All times are BJD-2454833.

Observed parameters			
Quantity	Best Fit	median	1 σ error
$LinearP_{01}$ [d]	114.73635	114.73631	± 0.00015
a_{01}/R_*	57.4	56.8	+1.4
r_{01}/R_*	0.06855	0.06859	-1.2
b_{01}/R_*	0.727	0.732	+0.00026
$LinearP_{02}$ [d]	191.2318	191.2315	-0.00028
a_{02}	80.7	79.9	+0.014
r_{02}/R_*	0.03123	0.03119	-0.017
b_{02}/R_*	0.579	0.591	+0.00015
P_{03} [d]	5.833904	5.833902	+2.0
$T_{mid,3}$ ^(a)	517.6762	517.6753	-1.7
a_{03}	7.88	7.80	+0.00041
r_{03}/R_*	0.00856	0.00853	-0.00042
b_{03}/R_*	0.567	0.591	+0.00042
P_{04} [d]	8.97741	8.97730	+0.025
a_{04}	10.50	10.40	-0.031
$T_{mid,4}$	519.4697	519.4679	+0.00050
r_{04}/R_*	0.00983	0.00925	-0.00059
b_{04}/R_*	0.746	0.742	+0.0047
Stellar parameters derived from spectroscopy			
M_* [M_\odot]	1.1		± 0.05
R_* [R_\odot]	1.82		± 0.04
Age [Gyr]	7 – 8		
Parameters from dynamical modeling			
Quantity	mean	median	1 σ error
M_* [M_\odot]	1.05	1.08	± 0.06
m_{01} [M_\oplus]	324.2	326.1	± 8.8
a_{01r} [AU]	0.471	0.474	± 0.010
P_{01} [d]	114.7309	114.7310	± 0.0005
e_{01}	0.036	0.039	± 0.009
ω_{01} [°]	238.6	255.3	± 27.6
M_{01} [°]	293.0	296.7	± 23.6
m_{02} [M_\oplus]	6.4	6.5	± 0.8
a_{02} [AU]	0.664	0.668	± 0.013
P_{02} [d]	192.363	192.389	± 0.074
e_{02}	0.039	0.042	± 0.012
ω_{02} [°]	223.2	240.1	± 18.8
M_{02} [°]	291.4	297.3	± 14.4
Derived physical parameters			
Quantity	Best Fit	median	1 σ error
r_{01} [R_\oplus]	13.49	13.49	± 0.55
a_{01} [AU] ^(b)	0.481	0.476	+0.026
i_{01} [°]	89.274	89.262	-0.028
ρ_{01} [$g\ cm^{-3}$]	0.729	0.728	+0.034
$T_{eq,01}$ [°K]	478.1	480.5	-0.030
r_{02} [R_\oplus]	6.14	6.14	± 0.29
a_{02} [AU] ^(b)	0.676	0.669	+0.037
i_{02} [°]	89.588	89.576	-0.040
ρ_{02} [$g\ cm^{-3}$]	0.152	0.153	+0.031
$T_{eq,02}$ [°K]	403.3	405.2	-0.027
r_{03} [R_\oplus]	1.68	1.68	± 0.17
a_{03} [AU] ^(b)	0.0660	0.0654	+0.0036
i_{03} [°]	85.87	85.66	-0.0039
$T_{eq,03}$ [°K]	1291	1297	+0.37
r_{04} [R_\oplus]	1.93	1.82	-0.45
a_{04} [AU] ^(b)	0.0880	0.0871	± 12
i_{04} [°]	85.93	85.91	± 0.19
$T_{eq,04}$ [°K]	1117.9	1123.3	+0.0048
			-0.0052
			+0.27
			-0.22
			± 10.0

notes:

- (a) A secondary solution, disfavored by $\Delta\chi^2 \approx 5$ is 517.6524
 (b) calculated using R_* times a_{XX}/R_* , not from dynamics

KOI 1574.03 and KOI 1574.04 have not been taken into account for the dynamical analysis.

Given the stellar mass from the spectral analysis as well as the orbital periods from the light curve, a reasonable set of start parameters can be estimated from the ratio of the TTV amplitudes and the phase of the TTV variations. From preliminary stability calculations the eccentricity could also be limited to be less or equal to about 0.1. We use the *IDL* routine *mpfit*, a Levenberg-Marquardt optimization, to fit the calculated transit timing variations as function of the stellar and the two planetary masses, the semi-major axes, eccentricities, lengths of periastron, as well as mean anomalies at $t = 0$. We then use this fit to generate 2500 random starting values within the error range provided by *mpfit* and converged them as well. From the resulting sample we derive histograms of for the parameters which allows to obtain mean values and uncertainties. Figures 5, 6, and 7 shows the resulting distribution of the stellar and the planetary masses.

We like to note that the mean stellar mass derived from the TTV analysis is close to the spectroscopic mass derived with the stellar density constraint (Sect. 2). The fit parameters are listed in Table 4. The mean masses for the two planets are $6.4 \pm 0.8 M_{\oplus}$ and $324.2 \pm 8.8 M_{\oplus}$ for the Kepler-87 c and b planets respectively. The bulk densities of the planets are determined to be $\rho_{01} = 0.729 \pm 0.026$ and $\rho_{02} = 0.152 \pm 0.019 \text{ g cm}^{-3}$, so the inner planet is a Jupiter mass planet with a Saturn-like density while the outer planet is a very low density planet in the super-Earth mass regime. The eccentricities are low, i.e. the 3σ errors are within the stable regime which allows eccentricities below about 0.1. Within the uncertainties, the lengths of peri-astron of the two orbits are aligned.

While the total number of measurements is larger than the free parameters, the number of TTV measurements for the outer planet (4) is low. The TTVs of the outer planet are mainly constraining by the mass of the inner planet (TTV amplitude), the eccentricity and periastron length of the outer planet (phase shift against TTV of inner planet and shape of TTV), by the mean anomaly of the outer planet (time of first transit) as well as by the mean orbital period of the outer planet. At first, it seems that the problem is over-determined, but these parameters are also constrained by the TTVs of the inner planet, however, more indirectly from the overall dynamical behavior of the three-body system. We therefore also analyzed the TTVs with a restricted set of parameters, i.e. we fixed the eccentricity and the length of periastron of the outer planet to their mean values. This does not change the results.

The deviations of the observed and simulated transit timings of the fit are presented in Fig. 3 and Fig. 4, the latter showing the residuals. The reduced χ^2 is 0.8. We also risk and attempt to predict the times of mid-transit for the next few years (see Table 3), but we note that the seemingly over-determined solution to Kepler-87 c make it difficult for us to put reliable error bars on the prediction. We do that mainly since comparing future observations of such timings with the predicted ones given in this paper are needed. This is quite likely, since the current observations cover the ≈ 550 days short term interaction cycle but do not cover the longer term interaction cycle of > 3000 days.

The minimum mutual Hill distance for the mean fit parameters is 4.7, which makes a long-term stable configuration plausible. Nevertheless, we integrated the orbit for 8 Gyr, i.e. the expected age of the system to ensure the dynamical stability, and found it to be stable.

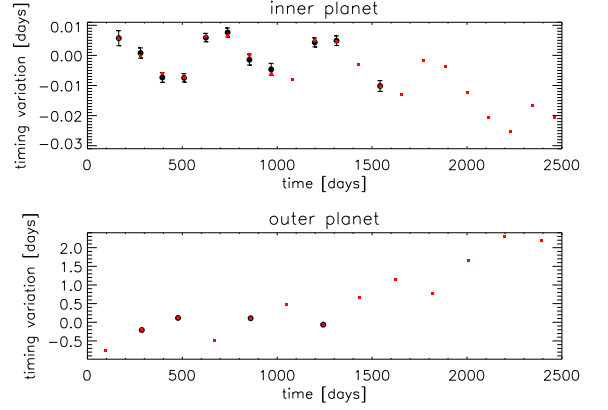


Fig. 3. Observed transit timing variations relative to a linear ephemeris (black) over plotted with the best model closest to the parameters of Table 4 (red squares). Top and bottom panels are for Kepler-87 b and c, respectively. The error bars for Kepler-87 c are smaller than the size of the symbols.

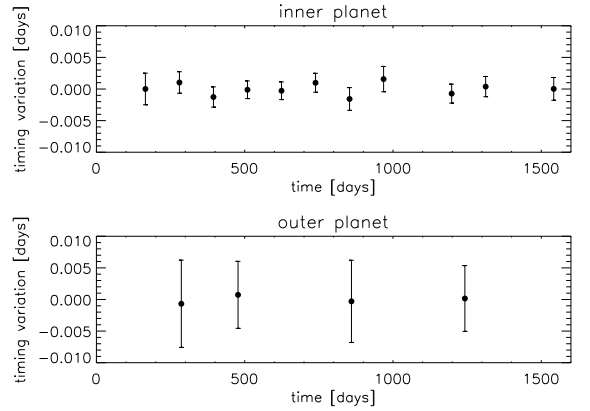


Fig. 4. Residuals between observed and calculated TTVs.

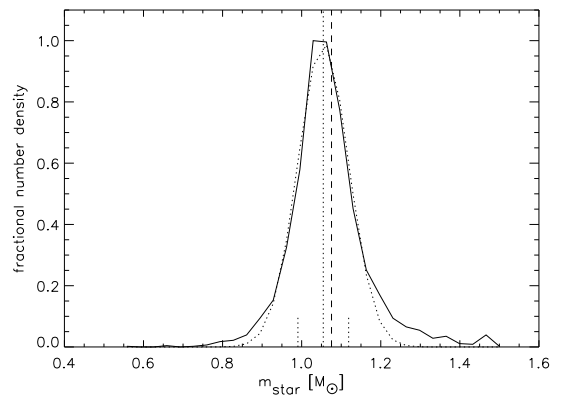


Fig. 5. Histogram of the stellar mass obtained from Levenberg-Marquardt fits starting at 2500 random initial values (full line) fitted with a Gaussian (dotted line). The mean (dotted) and the median (dashed) of the distribution are indicated as long vertical lines, the 1σ error as short vertical lines.

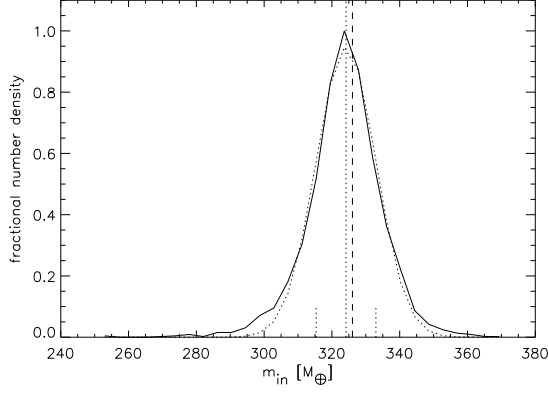


Fig. 6. Histogram of the mass of the inner planet obtained from Levenberg-Marquardt fits starting at 2500 random initial values (full line) fitted with a Gaussian (dotted line). The mean (dotted) and the median (dashed) of the distribution are indicated as long vertical lines, the 1σ error as short vertical lines.

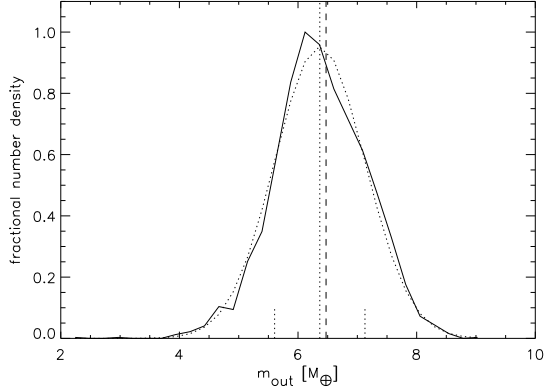


Fig. 7. Histogram of the mass of the outer planet obtained from Levenberg-Marquardt fits starting at 2500 random initial values (full line) fitted with a Gaussian (dotted line). The mean (dotted) and the median (dashed) of the distribution are indicated as long vertical lines, the 1σ error as short vertical lines.

5. Discussion

We presented the dynamical confirmation of two long period low-density transiting planets using transit timing variation, as well as the initial detection of two transiting super-Earth sized planet candidates, all in the Kepler-87 system. Kepler-87 c is the longest-period confirmed transiting planet around a single star, and Kepler-87 b has the third-longest period, after the previous record holder Kepler-30 d (Fabrycky *et al.* 2012). Batalha *et al.* (2013) strengthened the case for the paucity of short-period ($< 10d$) giant planets in multiple systems (Latham *et al.* 2011). However, this paucity seems to be less severe for longer periods giant planets such as Kepler-87 b. Particularly, the KOI 1574.04 planet candidate was not detected neither in the Q0-Q6 data (Batalha *et al.* 2013) nor in the Q1-Q12 data (Tenenbaum *et al.* 2012).

The most important feature of the Kepler-87 system is its two low density planets (Fig. 8). While Kepler-87 b ($\rho_{01} = 0.729 \pm 0.026$) has mass and radius that put it directly in the center of

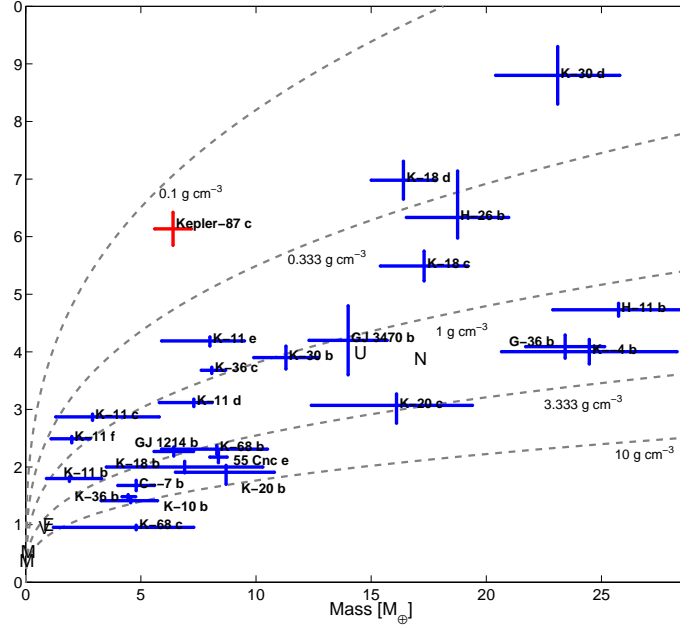


Fig. 8. Mass-radius relation for all known planets with masses below $30 M_{\oplus}$ with overplotted bulk density contours. It is obvious that Kepler-87 c occupies a unique position on this parameter space as the lowest-density planet for its super-Earth mass range. Some planet names were shortened so that “K-X” stands for the planet Kepler-X, and similarly “C-X” and “H-X” stand for “CoRoT-X” and “HAT-P-X”. Solar system planets are designated with a letter with no error bars. We note Kepler-87 b is beyond the scope of this figure (see discussion in the main text).

the general distribution of giant planets, Kepler-87 c ($\rho_{02} = 0.152 \pm 0.019$) is anomalously low-density for its mass, similar to that of the least dense very hot Jupiters (e.g. Hartman *et al.* 2011). However, the Kepler-87 planets are rarefied despite the fact that they are neither strongly irradiated nor young. Such low densities suggest that a significant mass fraction can be attributed to Hydrogen and Helium. While common for giant planets, such a composition is non-trivial for planets less massive than $10M_{\oplus}$ such as Kepler-87 c which at no point in its history had the canonical critical mass for the starting of gas accretion of $10M_{\oplus}$. Comparing these low densities to previously known planets is difficult since there are very few similarly long-period already include Kepler-35 b (Welsh *et al.* 2012) which has a density of $0.410^{+0.070}_{-0.069} g cm^{-3}$ - intermediate to the Kepler-87 planets. Importantly, there is no simple analogue to the low density of Kepler-87 c.

Initially this result seemed baffling to us. However, the above solution exhibits strong self-consistency between different determinations of some of the variables: the stellar mass from spectroscopy agrees with the stellar mass from dynamical modeling, and the semi-major axes from light curve fitting + stellar model agree with semi-major axes from dynamical model. From a theoretical stand point, Rogers *et al.* (2011) attempted to put limits on the masses of similarly-sized *Kepler* candidates and found that even low-mass low-density planets were possible in the general framework of core-nucleated accretion using plausible disc configurations. They found that a planet with a radius of $6R_{\oplus}$ like Kepler-87 c and an equilibrium temperature of $500^{\circ} K$

would have a mass of $6.4M_{\oplus}$ if $\approx 20\%$ of its mass were made of a gaseous envelope (assuming ice-rock interior, and H/He in protosolar proportions). Correcting for the lower equilibrium temperature of Kepler-87 c ($T_{eq} = 403.3$), its envelope mass fraction is probably somewhat higher than that. Planets such as Kepler-87 c, as well as the highly irradiated Kepler -11 and -36 systems (Lissauer *et al.* 2011 and Carter *et al.* 2012), demonstrate that the great compositional variety that was found for gas giants also extends down to planets with masses intermediate between Earth and Uranus.

We believe that the two large planets of the Kepler-87 system present an opportunity for detailed study of exoplanet interior structure: residing at a relatively large orbital distance they are significantly less affected by the extreme insolation, that on shorter period planets may produce inflated radii on the one hand and mass loss due to irradiation driven atmospheric escape on the other hand. Furthermore, the host star is at a stage of its evolution that is relatively age-sensitive, making the system age relatively well determined. This relatively benign and constrained environment should make the two planets more amenable to modeling.

The end of the Kepler mission also presents an interesting case where ground-based photometric follow-up of Kepler planets is very desirable: the systematic uncertainty associated with the low number of data points means that additional observations are of significant value. On the one hand, Kepler-87 b is an easy target (0.5% depth) to better Kepler's 2-plus-minutes timing precision, and almost any-precision detection of Kepler-87 c will be worthwhile due to its very large amplitude TTVs. On the other hand, due to their long periods and large host star both planets exhibit long transits of about 12hr and 15hr, which means full transits probably need a multi-site campaign. Note the accumulated effect of TTVs are very significant and can be even more than a day already in the near future (see Table 3).

6. Acknowledgements

A.O. acknowledges financial support from the Deutsche Forschungsgemeinschaft under DFG GRK 1351/2. M.Z. acknowledges support by the European Research Council under the FP7 Starting Grant agreement number 279347. We thank Guillem Anglada-Escudé for discussing at length this system with us. We thank Bill Cochran and the rest of his team who observed KOI 1574 and made the data available on CFOP. We would like to thank the team of the Hobby Eberly Telescope for taking the data of KOI 1574. This paper includes data collected by the Kepler mission. Funding for the Kepler mission is provided by the NASA Science Mission directorate. Some/all of the data presented in this paper were obtained from the Mikulski Archive for Space Telescopes (MAST). STScI is operated by the Association of Universities for Research in Astronomy, Inc., under NASA contract NAS5-26555. Support for MAST for non-HST data is provided by the NASA Office of Space Science via grant NNX09AF08G and by other grants and contracts. This research has made use of the NASA Exoplanet Archive, which is operated by the California Institute of Technology, under contract with the National Aeronautics and Space Administration under the Exoplanet Exploration Program.

References

- Anglada-Escudé, G., Arriagada, P., Vogt, S. S., et al. 2012, ApJ, 751, L16
 Batalha, N. M., Rowe, J. F., Bryson, S. T., et al. 2013, ApJS, 204, 24
 Bertelli, G., Girardi, L., Marigo, P., & Nasi, E. 2008, A&A, 484, 815
 Borucki, W. J., Koch, D. G., Batalha, N., et al. 2012, ApJ, 745, 120
 Carter, J. A., Agol, E., Chaplin, W. J., et al. 2012, Science, 337, 556
 Chambers, J. E. 1999, MNRAS, 304, 793
 Demarque, P., Woo, J.-H., Kim, Y.-C., & Yi, S. K. 2004, ApJS, 155, 667
 Fabrycky, D. C., Ford, E. B., Steffen, J. H., et al. 2012, ApJ, 750, 114
 Ford, E. B., Fabrycky, D. C., Steffen, J. H., et al. 2012, ApJ, 750, 113
 Hartman, J. D., Bakos, G. Á., Torres, G., et al. 2011, ApJ, 742, 59
 Holman, M. J., & Murray, N. W. 2005, Science, 307, 1288
 Howett, C. J. A., Spencer, J. R., Pearl, J., & Segura, M. 2010, Icarus, 206, 573
 Husser, T.-O., Wende-von Berg, S., Dreizler, S., et al. 2013, A&A, 553, A6
 Kim, Y.-C., Demarque, P., Yi, S. K., & Alexander, D. R. 2002, ApJS, 143, 499
 Latham, D. W., Rowe, J. F., Quinn, S. N., et al. 2011, ApJ, 732, L24
 Lissauer, J. J., Fabrycky, D. C., Ford, E. B., et al. 2011, Nature, 470, 53
 Mandel, K., & Agol, E. 2002, ApJ, 580, L171
 Ofir, A., Alonso, R., Bonomo, A. S., et al. 2010, MNRAS, 404, L99
 Ofir, A. 2013, A&A accepted, arXiv:1307.7330
 Ofir, A., & Dreizler, S. 2013, A&A, 555, A5
 Piskunov, N. E.; Valenti, J. A. 2002A&A...385.1095P
 Ramsey, L. W., Adams, M. T., Barnes, T. G., et al. 1998, Proc. SPIE, 3352, 34
 Rogers, L. A., Bodenheimer, P., Lissauer, J. J., & Seager, S. 2011, ApJ, 738, 59
 Savitzky, A., & Golay, M. J. E. 1964, Analytical Chemistry, 36, 1627
 Steffen, J. H., Fabrycky, D. C., Ford, E. B., et al. 2012, MNRAS, 421, 2342
 Stumpe, M. C., Smith, J. C., Van Cleve, J. E., et al. 2012, PASP, 124, 985
 Tegmark, M., Strauss, M. A., Blanton, M. R., et al. 2004, Phys. Rev. D, 69, 103501
 Tenenbaum, P., Jenkins, J. M., Seader, S., et al. 2012, arXiv:1212.2915
 Tull, R. G., MacQueen, P. J., Sneden, C., & Lambert, D. L. 1995, PASP, 107, 251
 Veverka, J., Helfenstein, P., Hapke, B., & Goguen, J. D. 1988, Mercury, University of Arizona Press, 37
 Welsh, W. F., Orosz, J. A., Carter, J. A., et al. 2012, Nature, 481, 475
 Yi, S., Demarque, P., Kim, Y.-C., et al. 2001, ApJS, 136, 417
 Yi, S. K., Kim, Y.-C., & Demarque, P. 2003, ApJS, 144, 259